

Tetramethylbenzidine-TetrafluoroTCNQ (TMB-TCNQF₄): A narrow-gap semiconducting salt with room temperature relaxor ferroelectric behavior

Stefano Canossa,¹ Elena Ferrari,² Pit Sippel,³ Jonas K. H. Fischer,^{3,4} Raphael Pfattner,⁵ Ruggero Frison,⁶ Matteo Masino,² Marta Mas-Torrent,⁵ Peter Lunkenheimer,³ Concepció Rovira,⁵ and Alberto Girlando^{*2,7}

¹EMAT, Department of Physics, University of Antwerp, 2020 Antwerp, Belgium

²Dipartimento di Scienze Chimiche, della Vita e della Sostenibilità Ambientale (S.C.V.S.A.) & INSTM-UdR Parma, Università di Parma, 43124 Parma, Italy

³Experimental Physics V, Center for Electronic Correlations and Magnetism, University of Augsburg, 86159 Augsburg, Germany

⁴Tohoku Forum for Creativity, Tohoku University, 980-8577 Sendai, Japan

⁵Department of Molecular Nanoscience and Organic Materials,

Institut de Ciència de Materials de Barcelona (ICMAB-CSIC) and Networking Research Center on Bioengineering, Biomaterials and Nanomedicine (CIBER-BBN), ES-08193 Bellaterra, Spain

⁶Physik-Institut, Universität Zürich, 8057 Zürich, Switzerland

⁷Present address: Molecular Materials Group, 43124 Parma, Italy

We present an extension and revision of the spectroscopic and structural data of the mixed stack charge transfer (CT) crystal 3,3',5,5'-tetramethylbenzidine-tetrafluoro-tetracyanoquinodimethane (TMB-TCNQF₄), associated with new electric and dielectric measurements. Refinement of synchrotron structural data at low temperature have led to revise the previously reported [Phys. Rev. Mat. **2**, 024602 (2018)] *C*2/*m* structure. The revised structure is *P*2₁/*m*, with two dimerized stacks per unit cell, and is consistent with the vibrational data. However, polarized Raman data in the low-frequency region also indicate that by increasing temperature above 200 K the structure presents an increasing degree of disorder mainly along the stack axis. This finds confirmation in the analysis of the anisotropic displacement parameters of the structure. TMB-TCNQF₄ is confirmed to be a narrow gap semiconductor ($E_a \sim 0.3$ eV) with room *T* conductivity of $\sim 10^{-4} \Omega^{-1} \text{cm}^{-1}$, while dielectric measurement have evidenced a typical relaxor ferroelectric behavior already at room *T*, with a peak in real part of dielectric constant $\epsilon'(T, \nu)$ around 200 K and 0.1 Hz. The relaxor behavior is explained in terms of the presence of spin solitons separating domains of opposite polarity that yield to ferroelectric nanodomains.

I. INTRODUCTION

Over the last few years, mixed-stack (ms) organic charge-transfer (CT) crystals have attracted great interest due to their unique properties of high tunability and promising applications in several fields of organic electronics, from Organic Field Effect Transistors (OFET) [1, 2], to photovoltaic devices [3], to organic ferroelectrics [4], and so on. In the case of binary molecular systems, ms CT crystals consist of a regular arrangement of face-to-face stacks of π -electron donor (D) and acceptor (A) molecular moieties with a defined stoichiometry. Such stacks are called mixed to distinguish them from segregated stacks of cation (D⁺) or anion (A⁻) radicals in other systems. The ionicity parameter ρ represents the degree of mixing between ground and excited CT state, and plays a fundamental role in the physical properties of ms CT crystals. The most common and most studied class of 1:1 ms CT crystals have a neutral or quasi-neutral ground state, $\rho \lesssim 0.5$. A handful have intermediate ionicity, and some of them upon lowering temperature or increasing pressure undergo a valence instability dubbed Neutral-Ionic transition [5]. Finally, the strongest electron Donor and Acceptor molecules form radical ion salts with $\rho \approx 1$, whose Madelung energy *M* exceeds the energy cost, *I* - *A*, to transfer an electron from D to A.

Mixed stack radical salts are rare, also because strong D and A molecules may prefer to crystallize as segregated stacks, as for instance DBTTF-TCNQF₄[6] or TMPD-TCNQF₄[7]. As a matter of fact, old literature search provided just four ionic ($\rho \geq 0.9$) ms CT crystals, namely, TMPD-TCNQ [8], M₂P-TCNQF₄[9], TTF-BA [10], and BEDO-TCNQCl₂ [11]. The three former all exhibit a spin Peierls transition around 200 K, 120 K and 50 K, respectively, whereas BEDO-TCNQCl₂ displays a first order transition around 100-120 K of unclear origin, but without stack dimerization.

More recently, some of us obtained another ionic ($\rho \simeq 0.9$) ms CT crystal, TMB-TCNQF₄, whose room *T* vibrational spectra clearly indicate a dimerized stack, whereas for X-ray the stack appeared as regular (equal distances between D and A) [12]. We have decided to further investigate this system, also including electric and dielectric measurements. Indeed, very little is known about semiconducting properties of ionic ms CT crystal. Furthermore, the above mentioned TTF-BA has been the first ms-CT crystal displaying ferroelectric properties in the low-*T* phase, where the stack is dimerized [13]. The new measurements reveal an actual dimerized stack structure already at room temperature *T*, with an intriguing relaxor ferroelectric behavior.

II. METHODS

A. Sample preparation

The crystals have been prepared by sublimation at about 180 °C in an open tube under controlled atmosphere [12], with a simplified version of the physical transport apparatus described by Laudise *et al.*[14].

B. Spectroscopic measurements

Polarized infrared (IR) absorption spectra of the crystals were recorded with a Bruker IFS-66 Fourier transform spectrometer coupled to the Hyperion 1000 IR microscope equipped with a wire-grid polarizer. Spectral resolution: 2 cm⁻¹. The Raman spectra with 752 nm excitation (Lexel Kr laser) were recorded with a Renishaw 1000 Raman spectrometer with the appropriate edge filter and coupled to a Leica M microscope. Raman with the other exciting lines were obtained with Horiba LabRAM HR Evolution spectrometer equipped either with a ULF Bragg filter or with the appropriate edge filter. Spectral resolution 2 cm⁻¹. Incident and scattered polarization was controlled by a half-wave plate and a thin-film linear polarizer, respectively, and the sample was rotated to record the different polarizations. A small liquid nitrogen cryostat (Linkam HFS 91) was used for temperature-dependent measurements under the IR and Raman microscopes.

C. Electric and dielectric measurements

Homogeneous thin single crystals of TMB-TCNQF₄ were analyzed under an optical microscope equipped with a polarizer/analyzer setup and electrostatically transferred Si/SiO₂ substrates with 200 nm thermally grown oxide thickness. Single crystals were electrically connected employing high conductive graphite paste (Dotite XC-12) and thin gold wires at the opposite tip of the needle-like crystals. Crystal dimensions were estimated using an optical microscope. Samples were prepared and electrically connected under ambient conditions (Relative humidity rH=40-60 % and temperature T = 28°C). All electrical characterization was carried out in darkness within an nitrogen filled glove box with low humidity and oxygen levels (H₂O < 2 ppm, and O₂ < 2 ppm) using a Keithley SourceMeter model 2612. Pseudo AC measurements at low current were used to prevent Joule heating of the sample (more detail in supporting information 15).

The dielectric constant and conductivity were determined using a frequency-response analyzer (Novocontrol Alpha-A). Gold wires were attached to contacts of gold paint on opposite tips of the needle-like crystals, ensuring an electric-field direction exactly parallel to the stack axis. Sample cooling and heating was achieved by a nitrogen-gas cryosystem (Novocontrol Quattro).

D. Structural measurements

To be completed.

III. RESULTS

A. Vibrational spectra

According to the reported crystal structure [12], at room temperature TMB-TCNQF₄ crystallizes in the monoclinic system $C2/m$ (C_{2h}^3), with two DA pairs per unit cell. All the molecules reside on inversion centers so that the stack appears to be regular. On the other hand, it has been already noted that the room temperature IR spectra polarized parallel to the stack are characterized by the presence of strong IR absorptions induced by the electron-molecular vibration (e-mv) coupling at the same frequencies of the main Raman bands [12]. This is an unquestionable hint of the loss of inversion center, i.e., the stack appears to be dimerized, in contrast to the X-ray crystal structure.

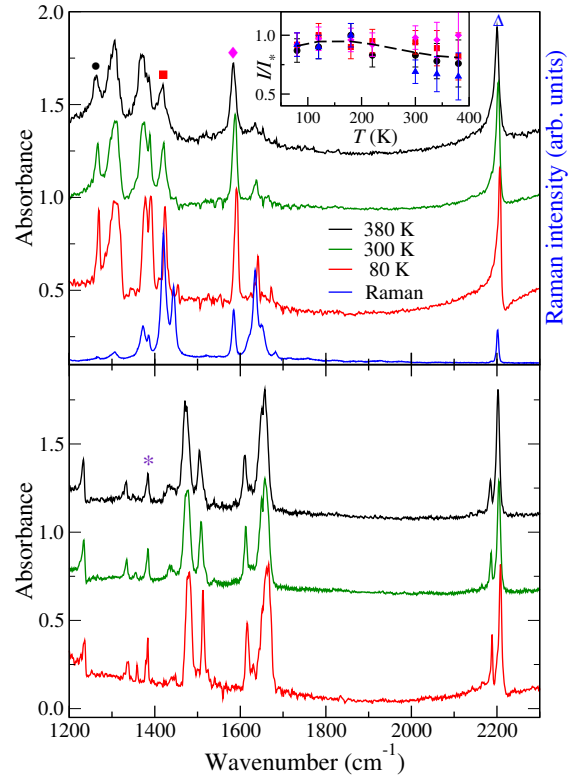


FIG. 1. Infrared spectra of TMB-TCNQF₄ as a function of T . Top panel: Spectra polarized parallel to the stack axis, compared with the Raman one (blue) to evidence the vibronic bands. Bottom panel: Spectra polarized perpendicular to the stack axis. Inset of top panel: T evolution of the ratio of the intensity of four e-mv induced bands (marked as black dot, red square, magenta diamond and blue triangle) with respect of a normally infrared active band (marked by an asterisk in the bottom panel).

There are several other cases of inconsistency between the results of X-ray and of vibrational spectroscopy, since the former probe long-range order and the latter the local (DA pair) structure. All these discrepancies have been explained in terms of some kind of disorder, either static or dynamic [8, 15–17]. Some hints about the presence of disorder may arise when looking at the temperature effects on the spectra.

With IR spectroscopy, we could go both above and below room temperature, as exemplified in Figure 1. No visually appreciable band intensity variations are detected between 380 and 80 K. To confirm this finding, we measured the relative intensity of four e-mv induced bands (marked in the top panel of the Figure as a black circle, a red square, a magenta diamond and a blue triangle) with respect to a normally IR active band detected in the spectrum polarized perpendicularly to the stack (marked by an asterisk in the bottom panel of the Figure). The results are plotted in the inset of Figure 1. The average relative intensity shows a slight increase around 220 K, but the change is well within the estimated error bars, that are larger at high T since the bands become broader. Therefore there is no clear evidence of a disorder-to-order transition by lowering T , as it happens in two other examples we are aware of [8, 16].

Raman spectroscopy in the low-frequency (10–200 cm^{-1}) region, involving lattice phonons, is known to be very sensitive to molecular packing [18] and also to disorder in a scale of a few unit cells [19], hence intermediate between the long-range order of X-ray and the local structure probed by high-frequency, intramolecular vibrations. We have thus obtained the low-frequency polarized Raman spectra of TMB-TCNQF₄ as a function of temperature shown in Figure 2.

The selection rules for TMB-TCNQF₄ Raman active lattice phonons in terms of the $C2/m$ (C_{2h}^3) factor group and adopting the rigid molecule approximations [20], are as follows: $2 A_g + 4 B_g$. So we expect only six bands, corresponding to the librations of the molecules, since the primitive cell contains just one DA pair, with each molecule on inversion center. A look at the experimental spectra shows that these spectral predictions are not obeyed, as there are more bands than expected. The highest frequencies bands, above 160 cm^{-1} , might also involve the methyl rotations, but even without counting them we observe eight bands, which become 10 at 80 K (Panel (a) of Fig. 2). Therefore the lattice mode spectral region, like that of the intramolecular vibrations, tells us that the previously reported space group [12] is not the correct one.

In addition, at room temperature the spectrum recorded with incident and scattered light polarized along the stack, labeled (\parallel, \parallel) , show two rather broad bands around 100 and 180 cm^{-1} , that by lowering T narrow and separate in more components, as detailed in panel (b) of the Figure. Notice also that the bandwidths observed in the other polarization are normal. This situation is reminiscent of what it has been observed in another CT

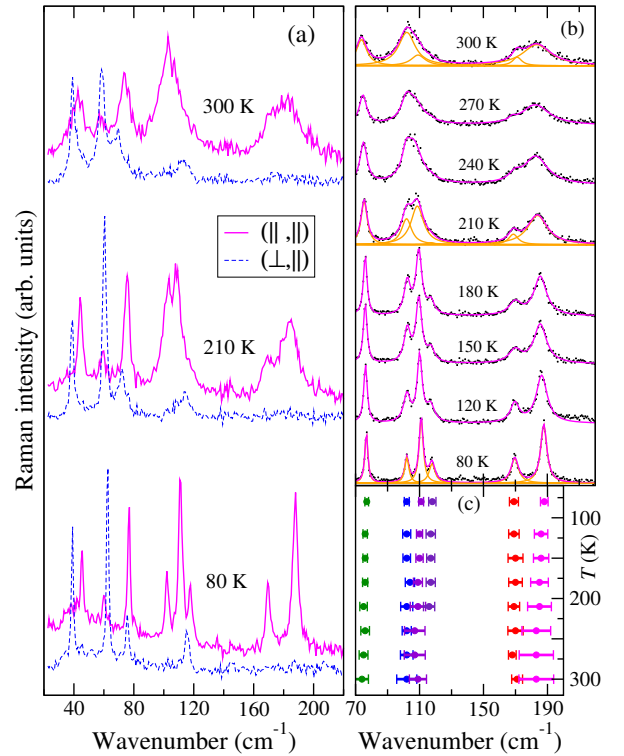


FIG. 2. Low-frequency Raman spectra as a function of temperature. (a) Spectra at three significant temperatures. The \parallel and \perp symbols within parenthesis indicate the polarization of incident and scattered light with respect to the stack axis. (b) Full T evolution of an enlarged portion of the (\parallel, \parallel) spectra. Black dots represent the experimental spectra, magenta lines the fitting with a set of Lorentzian functions. The single Lorentzians are reported as orange lines for the three most significant temperatures. (c) T evolution of the peak frequencies (dots) and of the corresponding FWHM (full width at half maximum, here represented as error bars) of the bands of panel (b).

crystal, M₂P-TCNQ [21]. In that case, the band broadening has been attributed to the electron-phonon coupling, since the broad bands also exhibit a marked frequency hardening by increasing the temperature, and their intensity is strongly enhanced by moving the frequency of the Raman exciting line towards the far-red, going into pre-resonance with the CT transition. Strong electron-phonon coupling means strong phonon anharmonicity, hence the line broadening.

To test if this explanation is valid also for TMB-TCNQF₄, we have followed in detail the temperature evolution of Raman bands in the (\parallel, \parallel) polarization, by performing a deconvolution in terms of Lorentzians, as exemplified for three temperatures by the orange lines in panel (b). Panel (c) summarizes such an analysis, in terms of the peak frequencies and Lorentzian FHMV, the latter represented by error bars. It is seen that the above-mentioned two groups of bands around 100 and 180 cm^{-1} start to separate around 200 K, but no anomalous frequency hardening is evident by lowering

the temperature. Furthermore, the spectra recorded by moving the exciting line toward the CT transition (see Supporting Information) show an intensity enhancement much less pronounced than in the case of M_2P -TCNQ [21]. Therefore in this case the remarkable band broadening and line merging observed by going towards room temperature is not due to the effect of electron-phonon coupling. In other words, whereas the band broadening observed in M_2P -TCNQ is mostly due to phonon anharmonicity, and is therefore ascribable to the so-called dynamic or thermal disorder, the analogous broadening we observe in TMB-TCNQF₄ must have a different origin. We believe it is due to disorder in the lattice structure along the stack axis, namely, to static, or displacement, disorder [22].

In summary, low-frequency Raman spectroscopy tells us that the space group symmetry is *lower* than that indicated by the refinement of the room temperature X-ray data [12], and that there is some kind of disorder along the stack.

B. Electric and dielectric measurements

As TMB-TCNQF₄ is a rare ionic mixed stack, we believed it was important to have a characterization of its electric and dielectric properties, by building transistors and condensers, as detailed in the Methods Section. Two crystals (sample 1, Fig. 13 and sample 2, Fig. 14) were measured and showed high source-drain currents (I_D) in FET measurements at low drain voltages with corresponding gate-leakage currents of at least two orders of magnitude smaller. No clear field-effect was observed in the applied voltage range, in contrast to what it has been recently reported by Uekusa et al. [23] with a series of TMB Acceptor CT crystals and films. Crystal bulk conductivity is probably dominant in the measured current, and the contribution of a possible thin-gate induced transistor channel at the dielectric/semiconductor interface is not clearly detectable. Estimated bulk conductivity values for sample 1 and sample 2 were $\sigma_1=4\cdot10^{-4}$ S/cm and $\sigma_2=2.2\cdot10^{-4}$ S/cm, respectively. The dc conductivity, measured at room T at low current, is around $3\cdot10^{-4} \Omega^{-1} \text{cm}^{-1}$. The T dependence of the conductance is reported for two samples in the top panels of Figure 3, and allows the extraction of the activation energy E_a , which turns out to be 0.32 – 0.33 eV, in agreement with Ref. [23].

The temperature dependence of the conductivity can also be obtained from low-frequency dielectric measurements, as reported in Fig. 4. At such low-frequency (0.1 Hz), $\sigma'(\omega, T)$ represents an estimate of the dc conductivity. At 300 K the conductivity value is around $9\cdot10^{-5} \Omega^{-1} \text{cm}^{-1}$, whereas the activation energy, estimated by applying the least square fitting to the linear part of the conductivity shown in Fig. 4, is 0.28 eV. In conclusion, both dc and low-frequency conductivity measurements classify TMB-TCNQF₄ crystal as a narrow-

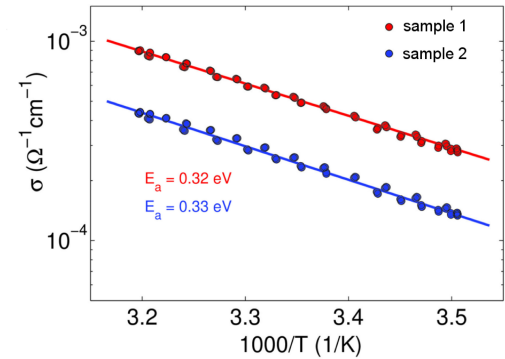


FIG. 3. Temperature dependence of the TMB-TCNQF₄ dc-conductivity obtained through transistor measurements.

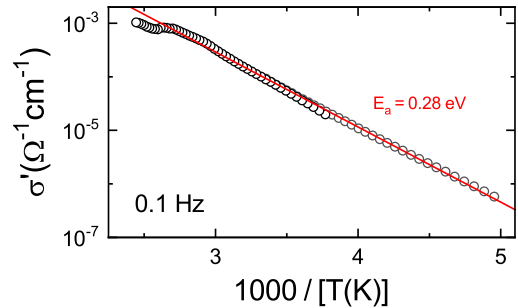


FIG. 4. Temperature dependence of the TMB-TCNQF₄ conductivity obtained by low-frequency dielectric measurements.

gap semiconductor ($E_a \sim 0.3$ eV), with a relatively high conductivity at room T ($\sim 10^{-4} \Omega^{-1} \text{cm}^{-1}$).

Additionally, the dielectric measurements as a function of T and frequency revealed a strange hysteretic behavior, as exemplified by the T dependence of the real (ϵ') and imaginary (ϵ'') parts of the dielectric constant at 259 Hz shown in Fig. 5. The minor anomalies observed in both quantities seem to look quite similar in two different samples, which is puzzling and speaks against a non-intrinsic origin. We do not have any evidence of a phase transition, and in any case the width of the hysteresis seems too large for a phase transition. We note, however, that the beginning of this “hysteresis” on cooling appears around the same temperature (≈ 250 K) as the starting of the disorder reduction seen in the low-frequency Raman spectra (Fig. 2) and in the possible slight intensity increase in the e-mv induced bands (inset of Fig. 1).

In the top panel of Fig. 6 the temperature-dependent real part of the dielectric constant is shown for frequencies between 0.1 Hz and 1.08 MHz. We observe large peaks in the permittivity, that decrease in amplitude and shift to higher temperature with increasing frequency. This corresponds to the typical behavior of relaxor ferroelectrics [24, 25]. Due to the needle-like geometry, the electrode area and thus the measured capacitance are very small, leading to a large uncertainty in the absolute

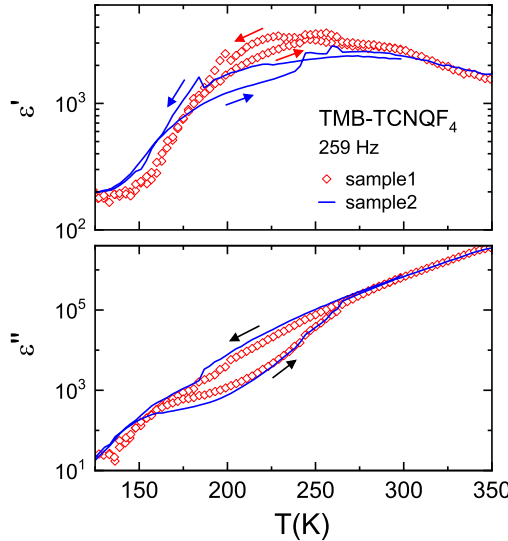


FIG. 5. Temperature dependence of the real and imaginary part of the dielectric constant of two TMB-TCNQF₄ samples at 259 Hz. The temperature cycle evidence a sort of hysteretic behavior between 270 and 170 K.

values of ϵ' . Finally, the dashed line in the top panel of Fig. 6 demonstrates that the right flanks of the relaxor peaks, representing the static dielectric constant, can be described by a Curie-Weiss law with a Curie-Weiss temperature of $T_{CW} \approx 202$ K, which provides an estimate of the quasi-static freezing temperature. The $\sigma'(T)$ plots reported in the bottom panel of Fig. 6 reveal indications of the loss peaks, expected for relaxors. Their right flanks are partly superimposed by the dc conductivity, approximated by the 0.1 Hz curve (cf. Fig. 4).

Frequency-dependent plots of the dielectric constant $\epsilon'(\nu)$ are shown in Fig. 7 for various temperatures. The spectra reveal a step-like decrease of $\epsilon'(\nu)$ which shifts to lower frequencies with decreasing temperature. This evidences the slowing down of relaxational dynamics with decreasing T . Similar to the peaks in $\epsilon'(T)$, the heights of the curves in $\epsilon'(\nu)$ decrease with increasing temperature, typical of relaxor ferroelectrics [24, 25].

To further analyze the relaxor dynamics, Fig. 8 presents an Arrhenius plot of the temperature-dependent relaxation times as determined from the fits shown in Fig. 7. The linear Arrhenius fit (line in the figure) yields an activation energy $E_a \sim 0.28$ eV, and a pre-exponential factor $\tau_0 = 5.9 \times 10^{-11}$ s. Similar Arrhenius behavior we have also observed for another organic relaxor, M₂P-TCNQ [21], whereas most, but not all, relaxor ferroelectrics can be described by the Vogel-Fulcher-Tammann law [26–28]. It is interesting to note that we have determined identical energy barriers for the dipole motion and the dc charge transport, indicating a close coupling of both dynamics.

Before closing this Section, a word of caution is necessary. In fact, one must be aware that a non-intrinsic, contact-related origin of the found relaxation process

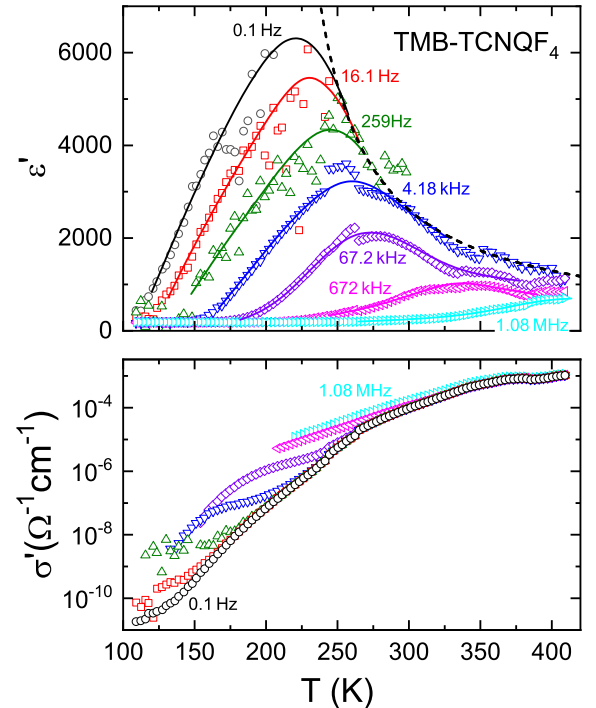


FIG. 6. Top panel: temperature dependence of the real part of the dielectric constant $\epsilon'(T)$. The solid lines are guides for the eyes. The dashed line demonstrates Curie-Weiss behavior with $T_{CW} = 202$ K. Bottom panel: temperature dependence of the frequency dependent conductivity $\sigma'(T)$.

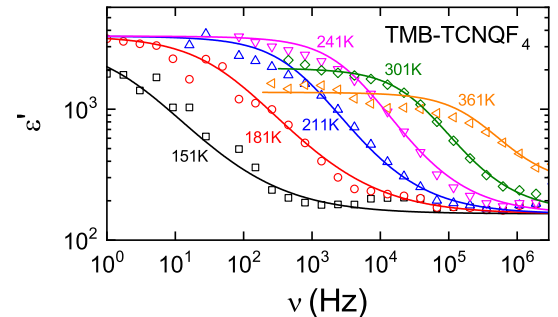


FIG. 7. Frequency-dependent plot of the dielectric constant $\epsilon'(\nu)$ of TMB-TCNQF₄ at various temperatures. Lines are fits with the Cole-Cole function.

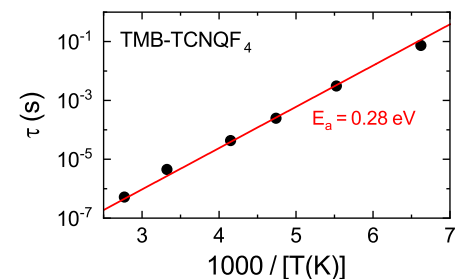


FIG. 8. Temperature evolution of TMB-TCNQF₄ relaxation time in an Arrhenius plot. The line shows an Arrhenius fit.

cannot be completely excluded. The usual tests to check for this effect, namely measurements with different sample geometries and with very different contact types cannot be easily done for the present needle-like, very brittle samples. Due to the sample geometry and the conductivity of the samples, we also cannot apply very high fields to check for hysteresis or polarization in the presumed relaxor ferroelectric state. However, the presence of (partially) ordered dipoles implied in a ferroelectric behavior is consistent with the lack of inversion center in the stack, as clearly indicated by vibrational spectroscopy.

C. Reanalysis of the crystal structure

In order to clarify the apparent contradiction between X-ray and spectroscopic/dielectric measurements, we decided to use synchrotron radiation at low T for a new structural analysis. The standard refinement process gave the centrosymmetric structure. However, a closer look at diffractograms evidenced weak, but clearly visible additional spots which violate the systematic absences predicted by the $C2/m$ space group. By including these spots, at 100 K the refinement converged to $P2_1/m$ with $R1\% = 4.4$, that with aspherical form factors and anisotropic hydrogen went down to 2.5. (Details are provided in the Supporting Informations). There are two stacks (two formula units) per unit cell, aligned along the a axis. The stacks are dimerized, with an inversion center between them, so that the dimers have anti-ferroelectric arrangement, as sketched in Fig. 9.

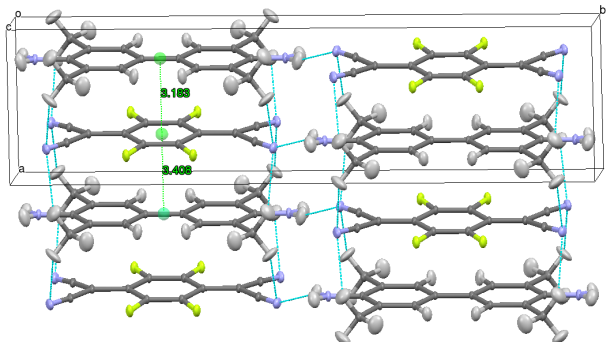


FIG. 9. Structure of TMB-TCNQF₄ at 100 K. The main hydrogen bonding and stacking distances (Å) between TMB and TCNQF₄ are shown.

Fig. 9 also evidences the presence of a network of hydrogen bonds between the methyl and the cyanide groups. These cooperate with the CT stacking interactions, whereas weaker contacts between the cyanide groups and the TMB aliphatic hydrogens connect the two stacks.

Intermolecular interactions have been also analyzed with the program Crystal Explorer in terms of electrostatic, polarization, dispersion, and exchange-repulsion interaction [29, 30], revealing the dominant role of intra-

column interactions in the overall lattice energy. The mean TMB-TCNQF₄ interaction energy is estimated to be -120.6 kJ/mol, approximately one order of magnitude higher than the remaining inter-column interactions (include a Table/Figure here or in the Supplementary Information).

Therefore the stack is dimerized, in agreement with spectroscopic measurements. However, since the primitive cell contains two stacks and an inversion center between the stacks, which then have an antiferroelectric arrangement. There is apparent contradiction with the dielectric measurements, since the relaxor behavior would imply at least ferroelectric domains. The disorder has to be analyzed by the the temperature evolution of anisotropic displacement parameters [31].

This part has to be completed.

IV. DISCUSSION AND CONCLUSIONS

The set of measurements presented here show that the physics of TMB-TCNQF₄ is quite interesting and peculiar, but also rather complex, so that its understanding still awaits additional sophisticated experiments and proper modeling. It has been shown that TMB-TCNQF₄ is a narrow gap semiconductor ($E_a \simeq 0.3$ eV), with an optical gap of about 0.8 eV, and a quasi ionic ground state ($\rho \simeq 0.9$) [12]. The most important advancement of the present study with respect to the previous ones [12, 23] consists in the finding that TMB-TCNQF₄ stacks are dimerized, and that some kind of disorder along the stacks is present above ≈ 200 K. However, the passage from the disordered to the ordered structure takes ≈ 100 K (Figs. 1, 2 and 5), and does not look like a real phase transition. The room T conductivity is relatively high ($\sim 10^{-4} \Omega^{-1} \text{ cm}^{-1}$), and decreases by three orders of magnitude in going to 200 K. Finally, relaxor-ferroelectric-like behavior has been observed already at room temperature, with a maximum in $\epsilon'(\nu, T)$ around 200 K and 0.1 Hz (top panel of Fig. 6). The relaxor behavior is consistent with the disorder, but not with the anti-ferroelectric arrangements of the two stacks in the unit cell.

Modeling of TMB-TCNQF₄ physical properties in terms of a Peierls-Hubbard model and/or band structure relevant to a regular, ordered stack is clearly inappropriate [12, 23]. Electrical properties have to take into account the gap opening due to dimerization and the effect of disorder. Band structure calculations (Supplementary information, to be introduced) indeed show that the gap is due to dimerization and not to electron-electron interactions. Moreover, first principle calculations have problems also for a perfectly ordered structure, since, as we have tried, they do not reproduce the observed charge separation. However, at the present stage we can envision a quite plausible scenario able to reconcile all the presently available experimental data, giving directions for future investigations.

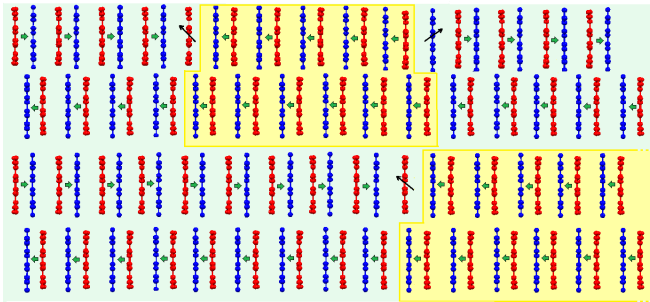


FIG. 10. Illustration of how the presence of spin solitons in TMB-TCNQF₄ yields ferroelectric domains (pale yellow regions) inside a otherwise anti-ferroelectric arrangement (light green regions). Blue molecules: TMB; red molecules: TCNQF₄. The dimerization is amplified for clarity. The green bold arrows indicate the direction of the electric dipole within the dimer, whereas the spin soliton is indicated by an inclined black arrow on the molecule.

Analysis of the low T structures of TMB-TCNQF₄ has shown that the system is strongly 1D, with the TMB and TCNQF₄ molecules perfectly aligned on top of each other along the stacks, and weak inter-stack interactions. In going above ≈ 200 K, the structure becomes disordered *along* the stack, as shown by the low-frequency Raman spectra. This kind of disorder is most likely displacive, and adds to the usual thermal disorder.

As we stated in the Introduction, 1D systems like the present one are subject to the spin-Peierls instability, which is the driving force of the dimerization. However, it is also well known that in strictly 1D systems phase transitions are not allowed down to 0 K, and that fluctuations are present until 3D interactions become significant [32]. In TMB-TCNQF₄ the dimerization is probably also affected by the methyl-nitrogen contacts, (see Figure) but here we are proposing a rather simplified general scenario. Fluctuations involve “defects” of dimerization, boundaries between domains of different orientation, namely the spin solitons depicted in Fig. 10. At room T the disorder is likely due to presence of nanoscopic domains, which are able to move under the effect of the electric field. And there is no correlation between domains in different chains, so that we have the possibility of ferroelectric regions (indicated in pale yellow in the Figure) inside an anti-ferroelectric structure. In this model, these ferroelectric nanodomains are the origin of the relaxor behavior, in accord with the common explanation of relaxor ferroelectricity by nanoscale ferroelectric order [24, 25]. By lowering T , the population of solitons decreases, namely, the dimension of ferroelectric domains increases and their motions under the electric

field becomes slower and slower until the electrostatic interactions and inter-chain hydrogen-nitrogen contacts lock the chains into the fully ordered anti-ferroelectric $P2_1/m$ structure.

Besides polyacetylene [33], spin solitons have been detected and widely studied in the CT crystal Tetrathiafulvalene-Chloranil (TTF-CA) and derivatives in their low temperature or high pressure (p) dimerized stack phase [34–36]. Although the present data do not fully prove it, the above scenario is then quite plausible, suggesting a wide playground of new experiments and theory, perhaps more promising than that of TTF-CA. In fact, whereas in TTF-CA the studies have to be performed at low T or high p , here solitons are possibly present at ambient conditions. Since TMB-TCNQF₄ is quasi-ionic, triplet spin excitations are likely thermally populated and easily experimentally accessible. Proper characterization of the disorder, for instance by neutron diffraction, would allow to establish the correlation length, or dimensions of the differently oriented nanodomains, which would provide the basis for a better understanding of the still rather mysterious relaxor ferroelectric behavior. Efforts should be also devoted to the growth of the crystals by different methods, possibly in the form of thin films. If successful, TMB-TCNQF₄ might be interesting even from the perspective of materials application. In fact, the dimerized phase of TTF-CA has a ferroelectric arrangement, and poling yields to an ordered phase with ferroelectric hysteresis [37]. In TMB-TCNQF₄ the ordered state is anti-ferroelectric, but the ferroelectric domains would offer the possibility of building a room T relaxor ferroelectric [38].

ACKNOWLEDGMENTS

AG thanks Prof. Pascale Foury-Leykleian for very helpful discussions about the crystallographic issues. JKHF and PL acknowledge funding from the Deutsche Forschungsgemeinschaft (DFG) via the Transregional Collaborative Research Center TRR80 (Augsburg, Munich). R.P. and M.M.-T. acknowledge support from the Marie Curie Cofund, Beatriu de Pinós Fellowships (Grant Nos. AGAUR 2017 BP 00064). This work was also supported by the Spanish Ministry project GENESIS PID2019-111682RB-I00, the “Severo Ochoa” Programme for Centers of Excellence in R&D (FUN-FUTURE, CEX2019-000917-S) and the Generalitat de Catalunya (2017-SGR-918). In Parma the work has benefited from the equipment and support of the COMP-HUB Initiative, funded by the “Departments of Excellence” program of the Italian Ministry for Education, University and Research (MIUR, 2018–2022).

[1] J. Zhang, J. Jin, H. Xu, Q. Zhang, and W. Huang, *J. Mater. Chem. C* **6**, 3485 (2018).

[2] T. Salzillo, C. A., and M.-T. M., *J. Mater. Chem. C* **7**, 10257 (2019).

- [3] S. J. Kang, S. Ahn, J. B. Kim, C. Schenck, A. M. Hiszpanski, S. Oh, T. Schiros, Y.-L. Loo, and C. Nuckolls, *Journal of the American Chemical Society* **135**, 2207 (2013).
- [4] S. Horiuchi, K. Kobayashi, R. Kumai, and S. Ishibashi, *Chemistry Letters* **43**, 26 (2014).
- [5] M. Masino, N. Castagnetti, and A. Girlando, *Crystals* **7**, 108 (2017).
- [6] T. J. Emge, W. A. Bryden, F. M. Wiygul, D. O. Cowan, T. J. Kistenmacher, and A. N. Bloch, *The Journal of Chemical Physics* **77**, 3188 (1982).
- [7] M. Meneghetti, R. Bozio, C. Bellitto, and C. Pecile, *The Journal of Chemical Physics* **89**, 2704 (1988).
- [8] A. Girlando, A. Painelli, and C. Pecile, *Molecular Crystals and Liquid Crystals* **112**, 325 (1984).
- [9] M. Meneghetti, A. Girlando, and C. Pecile, *The Journal of Chemical Physics* **83**, 3134 (1985).
- [10] A. Girlando, C. Pecile, and J. Torrance, *Solid State Communications* **54**, 753 (1985).
- [11] T. Hasegawa, T. Mochida, R. Kondo, S. Kagoshima, Y. Iwasa, T. Akutagawa, T. Nakamura, and G. Saito, *Phys. Rev. B* **62**, 10059 (2000).
- [12] N. Castagnetti, M. Masino, C. Rizzoli, A. Girlando, and C. Rovira, *Phys. Rev. Materials* **2**, 024602 (2018).
- [13] F. Kagawa, S. Horiuchi, M. Tokunaga, J. Fujioka, and Y. Tokura, *Nature Physics* **6**, 169 (2010).
- [14] R. Laudise, C. Kloc, P. Simpkins, and T. Siegrist, *Journal of Crystal Growth* **187**, 449 (1998).
- [15] A. Girlando, A. Painelli, and C. Pecile, *The Journal of Chemical Physics* **89**, 494 (1988).
- [16] S. A. Bewick, R. A. Pascal, D. M. Ho, Z. G. Soos, M. Masino, and A. Girlando, *Journal of Chemical Physics* **122**, 1 (2005).
- [17] M. Kumar, B. J. Topham, R. Yu, Q. B. D. Ha, and Z. G. Soos, *The Journal of Chemical Physics* **134**, 234304 (2011).
- [18] A. Brillante, I. Bilotti, R. G. D. Valle, E. Venuti, and A. Girlando, *CrystEngComm* **10**, 937 (2008).
- [19] A. Brillante, I. Bilotti, R. G. Della Valle, E. Venuti, A. Girlando, M. Masino, F. Liscio, S. Milita, C. Albonetti, P. D'Angelo, A. Shehu, and F. Biscarini, *Physical Review B - Condensed Matter and Materials Physics* **85**, 1 (2012).
- [20] G. Turrell, *Infrared and Raman Spectra of Crystals* (Academic Press, 1972) Chap. 4-6.
- [21] J. K. H. Fischer, G. D'Avino, M. Masino, F. Mezzadri, P. Lunkenheimer, Z. G. Soos, and A. Girlando, *Physical Review B* **103**, 115104 (2021).
- [22] A. Guinier, *X-Ray Diffraction* (W.H. Freeman and Co., San Francisco and London, 1963) Chap. 6.
- [23] T. Uekusa, R. Sato, D. Yoo, T. Kawamoto, and T. Mori, *ACS Applied Materials & Interfaces* **12**, 24174 (2020).
- [24] L. E. Cross, *Ferroelectrics* **76**, 241 (1987).
- [25] G. A. Samara, *Journal of Physics: Condensed Matter* **15**, R367 (2003).
- [26] H. Vogel, *Zeitschrift für Physik* **22**, 645 (1921).
- [27] G. S. Fulcher, *Journal of the American Ceramic Society* **8**, 339 (1925).
- [28] G. Tammann, *Annalen der Physik* **307**, 1 (1900).
- [29] M. J. Turner, S. Grabowsky, D. Jayatilaka, and M. A. Spackman, *The Journal of Physical Chemistry Letters* **5**, 4249 (2014).
- [30] J. W. S. G. D. S. P. J. D. S. M. Turner, M.J; McKinnon, *Crystal explorer 17* (2017).
- [31] H. B. Bürgi and S. C. Capelli, *Acta Crystallographica Section A* **56**, 403 (2000).
- [32] P. Pincus, Basic principles and concepts in the physics of low dimensional cooperative systems, in *Low-Dimensional Cooperative Phenomena*, NATO ASI B, Vol. 7, edited by H. J. Keller (Springer US, 1975) Chap. 1.
- [33] A. J. Heeger, S. Kivelson, J. R. Schrieffer, and W. P. Su, *Reviews of Modern Physics* **60**, 781 (1988).
- [34] F. Kagawa, S. Horiuchi, H. Matsui, R. Kumai, Y. Onose, T. Hasegawa, and Y. Tokura, *Phys. Rev. Lett.* **104**, 227602 (2010).
- [35] K. Sunami, T. Nishikawa, K. Miyagawa, S. Horiuchi, R. Kato, T. Miyamoto, H. Okamoto, and K. Kanoda, *Science Advances* **4**, 1 (2018).
- [36] Z. G. Soos and A. Painelli, *Physical Review B* **75**, 1 (2007).
- [37] K. Kobayashi, S. Horiuchi, R. Kumai, F. Kagawa, Y. Murakami, and Y. Tokura, *Physical Review Letters* **108**, 1 (2012).
- [38] C. W. Ahn, C.-H. Hong, B.-Y. Choi, H.-P. Kim, H.-S. Han, Y. Hwang, W. Jo, K. Wang, J.-F. Li, J.-S. Lee, and I. W. Kim, *Journal of the Korean Physical Society* **68**, 1481 (2016).

SUPPORTING INFORMATION

Raman spectra with different exciting lines

Room temperature polarized Raman spectra were collected with different excitation lines (from 633 to 1064 nm) to investigate the intensity enhancement in approaching the CT transition, located at 6500 cm^{-1} (0.81 eV)[12]. Figure 11 shows that in the (\parallel, \parallel) polarization (red lines) the low-frequency modes are clearly enhanced with respect to the intra-molecular modes and low-frequency modes in the (\perp, \perp) polarization (blue lines). However, this resonance effect is considerably lower than that observed in the previously studied dimerized stack CT crystal M₂P-TCNQ.[21]

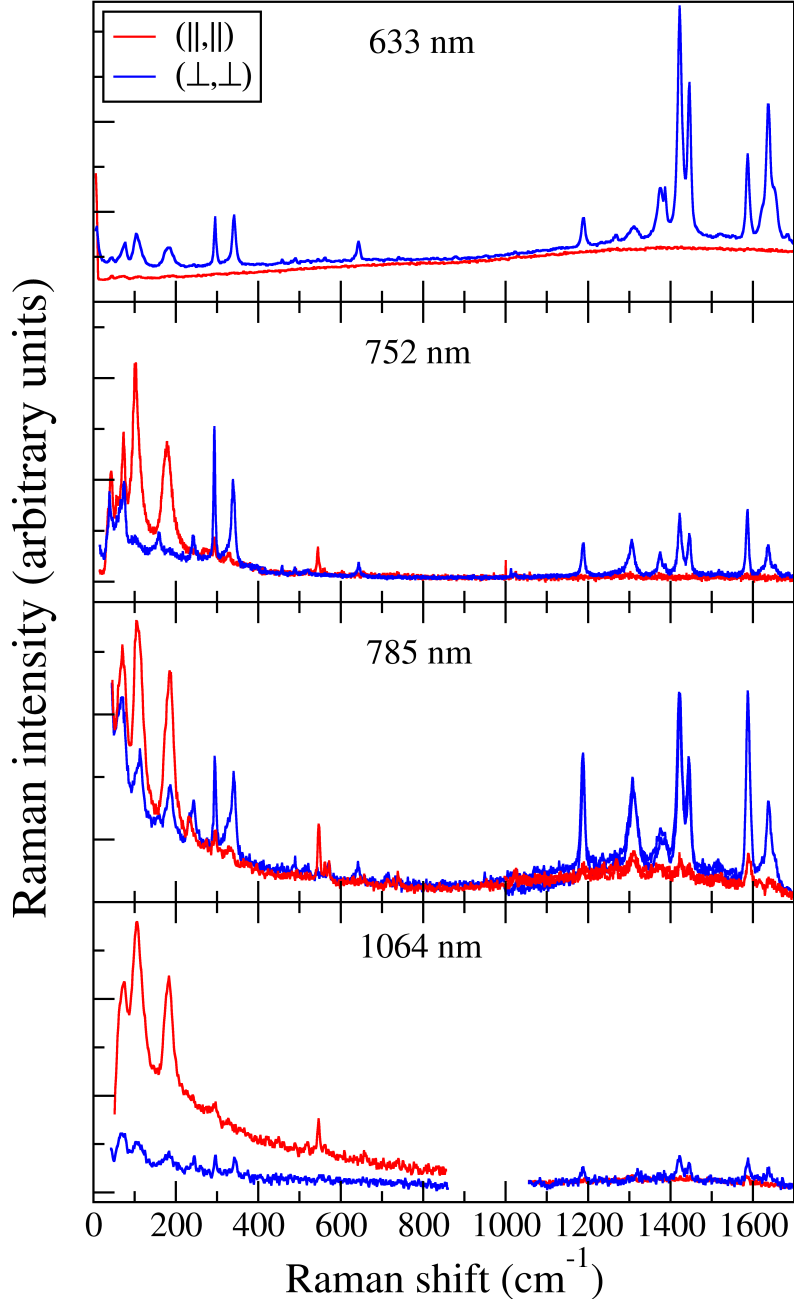


FIG. 11. Polarized Raman spectra of TMB-TCNQF₄ as a function of the laser exciting line. Red lines: Incident and scattered radiation polarized parallel to the stack axis; Blue line: Incident and scattered radiation polarized perpendicular to the stack axis.

In order to better justify the above assertion, in Fig. 12 we have plotted for both compounds the intensity of one low-frequency mode in the (\parallel, \parallel) polarization with respect to the intensity of a nearby mode in the (\perp, \perp) polarization, which is not affected by resonance with the CT transition. It is seen that with excitation in the red (≈ 1.6 eV) the enhancement for M_2P -TCNQ is about five times as large as that of TMB -TCNQF₄, although the excitation line is more close to the CT transition energy (dotted lines in the left of the Figure).

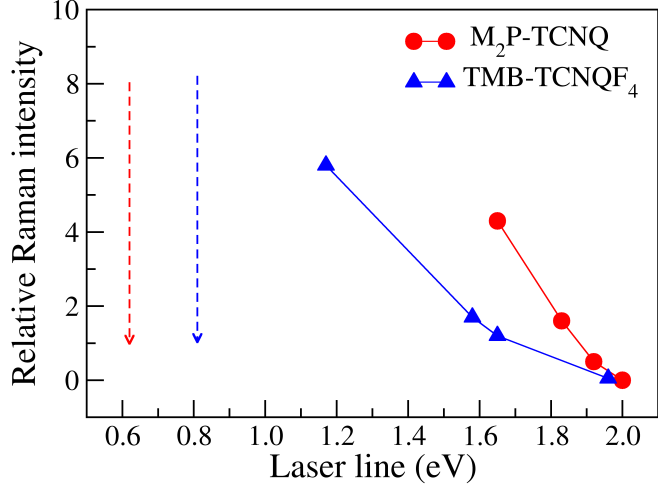


FIG. 12. Blue triangles: Relative Raman intensity of the TMB -TCNQF₄ 103 cm^{-1} band in the (\parallel, \parallel) polarization with respect to the 292 cm^{-1} one in the (\perp, \perp) polarization, as a function of the laser exciting line (expressed in eV). Red circles: Relative Raman intensity of the M_2P -TCNQ 125 cm^{-1} band in the (\parallel, \parallel) polarization with respect to the 320 cm^{-1} one in the (\perp, \perp) polarization [21]. The vertical blue and red dotted lines on the left indicate the CT frequency of the two crystals.

FET measurements

Figure 13 and 14 show the FET output characteristics measured for two single crystals of TMB-TCNQF₄ namely sample 1 and sample 2.

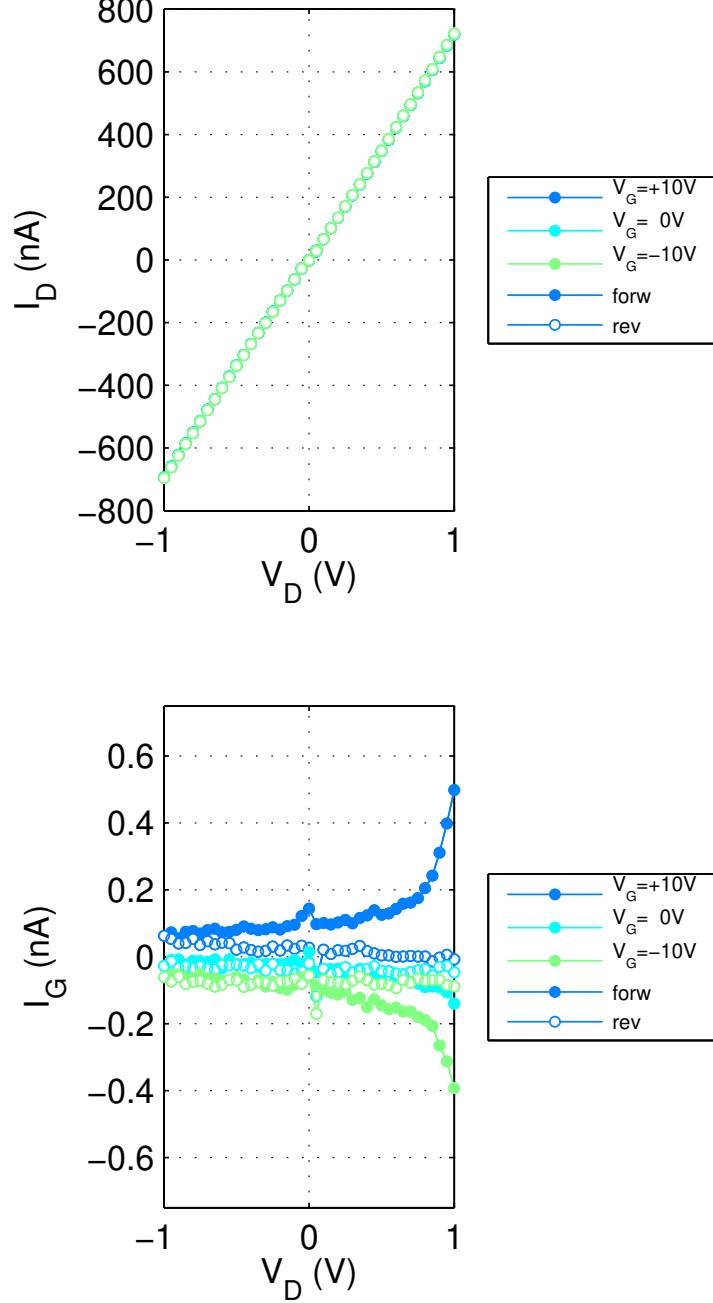


FIG. 13. Field-Effect transistor output characteristics ($I_D(V_D)$) of sample 1 including leakage currents ($I_G(V_D)$) both in forward and reverse drain voltage sweeps.

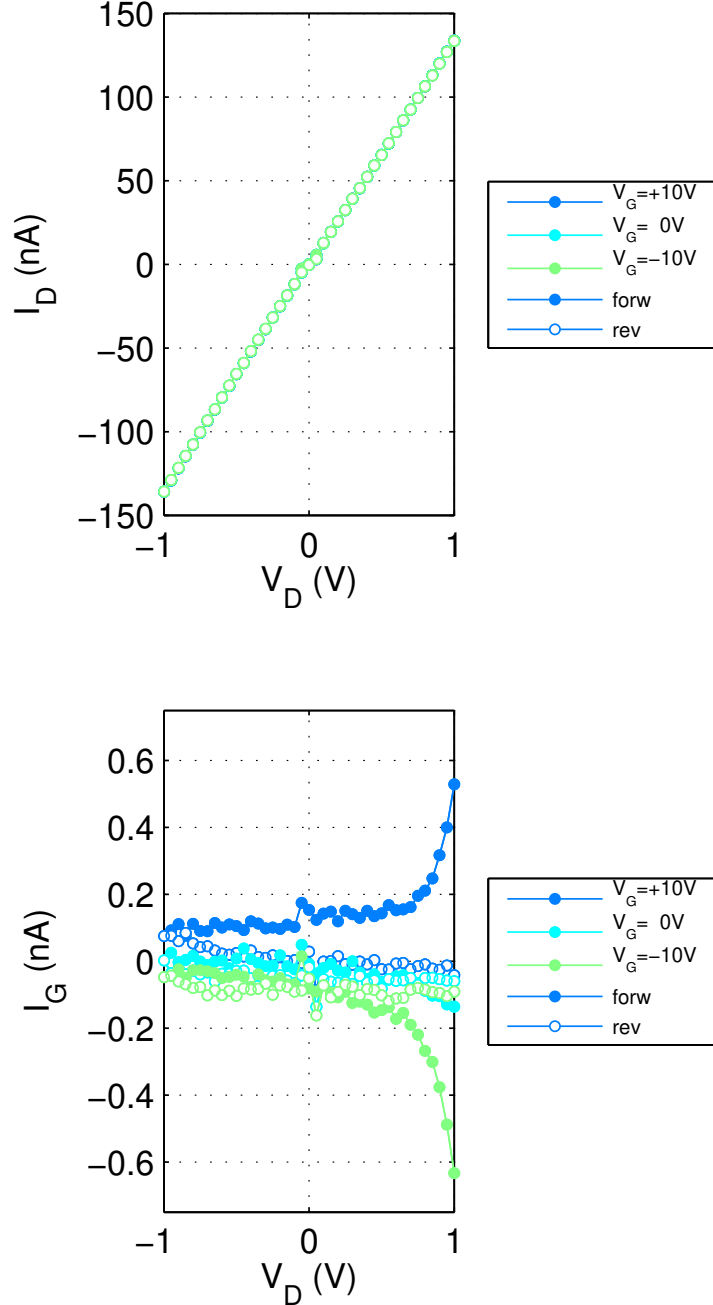


FIG. 14. Field-Effect transistor output characteristics ($I_D(V_D)$) of sample 2 including leakage currents ($I_G(V_D)$) both in forward and reverse drain voltage sweeps.

Pseudo AC conductivity measurements

To extract the temperature dependence of TMB-TCNQF₄ single crystals, the substrates were mounted to an aluminum frame equipped with a Peltier element. Temperature was monitored in real-time using a calibrated Pt₁₀₀₀ sensor. First and second order temperature resistance coefficients were extracted for both crystals using equation 1 exhibiting $\alpha=-9.13$ (%/K) and $\beta=0.10$ (%/K²), respectively, as illustrated in Fig. 15.

$$R(T) = R_{T_0} \cdot [1 + \alpha(T - T_0) + \beta(T - T_0)^2] \quad (1)$$

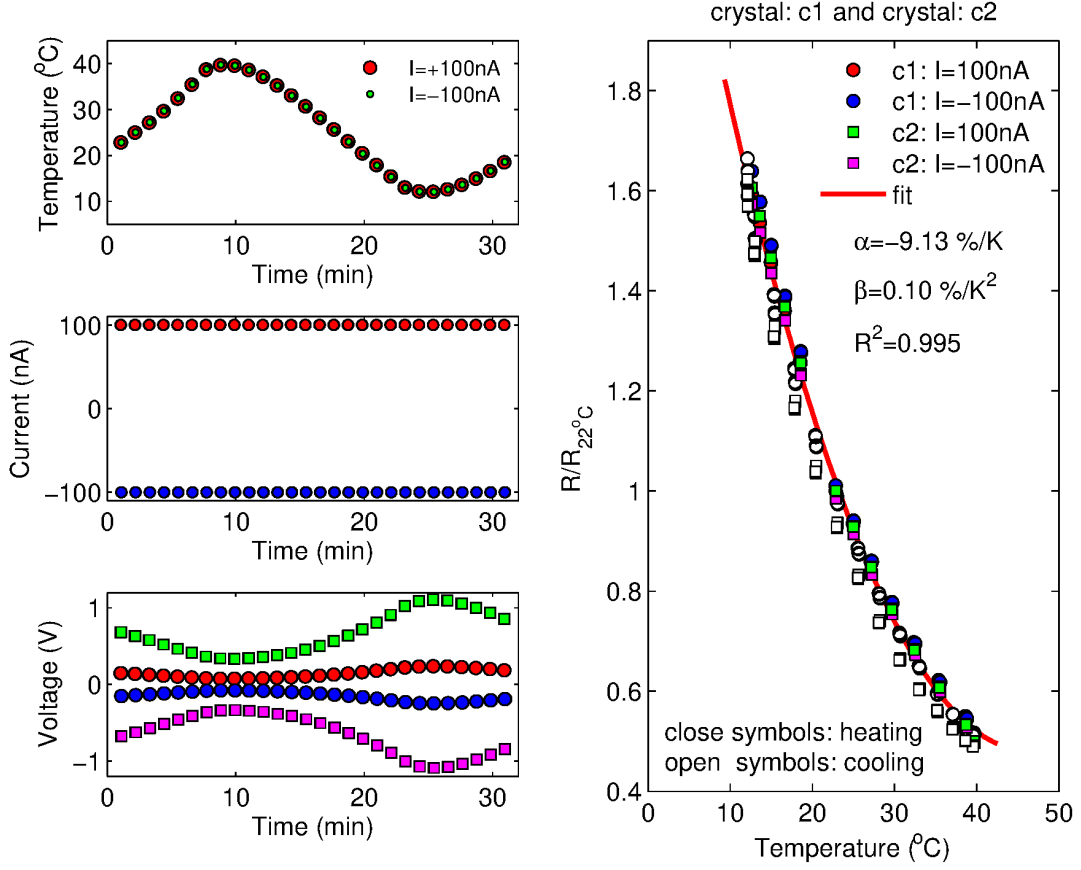


FIG. 15. Temperature dependence of two TMB-TCNQF₄ crystals employing pseudo AC current of $I = \pm 100$ nA while measuring two probe resistance. a) Temperature ramp starting at room temperature heating up to $T=40^\circ\text{C}$ followed by cooling ramp down to $T=10^\circ\text{C}$ and back to room temperature. b) Applied current values to both crystals and c) measured voltage values. d) Calculated electrical resistance ($R/R_{22^\circ\text{C}}$) as function of temperature for both crystals including heating (closed symbols) and cooling (open symbols) cycles. Red curve fit for the extraction of first and second order temperature coefficients, α and β , respectively.

The activation energy was extracted using equation 2 giving values of $E_a=0.32$ eV and $E_a=0.33$ eV, for sample 1 and sample 2, respectively.

$$\sigma = \sigma_0 \cdot e^{-\frac{E_a}{k_B T}} \quad (2)$$